SURCOS: a software tool to simulate irrigation and fertigation in isolated furrows and furrow networks

J. Burguete[a,c,*], A. Lacasta[b], P. García-Navarro[b]

[a]Soil and Water, EEAD / CSIC. P.O. Box 13034, 50080 Zaragoza, Spain.
[b]Fluid Mechanics, LIFTEC, CSIC-Universidad de Zaragoza. María de Luna 3, 50018 Zaragoza, Spain.
[c]BIFI: Instituto de Biocomputación y Física de Sistemas Complejos, Universidad de Zaragoza. Mariano Esquillor, Edificio I+D, 50009 Zaragoza, Spain.

Abstract

A software tool useful for the numerical computation of surface irrigation and fertigation in furrows and furrow networks was developed. The model solves the complete one-dimensional St-Venant equations together with the transport equation of a passive solute. The flow equations and the solute advection are solved with a high resolution TVD explicit Eulerian scheme. The solute dispersion is solved with a centered implicit Eulerian scheme to avoid further restriction in the allowable time step. The computational speed of the model is high in isolated furrows. In cases of large furrow networks over extended irrigation times the model is slower but affordable computational speed is achieved. The computational model has been designed to be robust, intuitive and able to supply useful visual results. Both the executable and the source code, as well as the examples presented can be downloaded, edited and distributed under a BSD type license.

Keywords: simulation software, infiltration, furrows, irrigation, fertigation

1. Introduction

Engineering studies of surface irrigation systems begin with an evaluation of current performance based on field-measured data in order to determine the applied amount of the irrigation water. The interest is in the distribution of infiltrated water along the field in order to evaluate whether water contributed

*Corresponding author
Email addresses: jburguete@eead.csic.es (J. Burguete), alacasta@unizar.es (A. Lacasta), pigar@unizar.es (P. García-Navarro)

to satisfy the irrigation requirement and how much was lost by deep percolation and runoff. The ultimate objective is to identify recommendations that result in acceptable levels of irrigation performance under the expected range of field conditions.

In the last decades computer based models were developed to support this analytical process. The most usual simulation engines, WinSRFR (Clemmens and Strelkoff, 1999) and SIRMOD (Walker, 2003), can be configured to model basins, borders, and furrows, all under the assumption of one-dimensional flow. This means that all flow characteristics vary only with distance along the field length and time, i.e. not across the field width. For borders and basins, the models are applicable to situations where the side-fall is negligible in comparison with the applied depth, infiltration and roughness are relatively uniform across the field width, and inflow is distributed. With furrows, simulations consider only a single furrow and, therefore, neighboring furrows are assumed identical. Any variation in properties from furrow to furrow must be modeled separately. Their simulation engines solve the one-dimensional unsteady open-channel flow equations coupled with empirical/semi-empirical equations describing infiltration and channel roughness. The governing equations represent the physical principles of conservation of mass and momentum. Given the relatively low velocities and Froude numbers that characterize surface-irrigation flows, their simulation engines often solve truncated forms of the momentum equation. The zero-inertia (force equilibrium) version assumes only pressure gradients, friction, and gravitational forces acting on the flow. Examples of recent applications of these models can be Bautista et al. (2009b,a) or Ebrahimiam and Liaghat (2011). It is difficult to find published, easy and user friendly software tools based on other similar models as, for instance, Mailapalli et al. (2009) or Soroush et al. (2013).

Water flow simulation in open channels and rivers has been a topic of interest recently and many numerical advances can be found. They include the presence of transcritical flow, bed slope changes, non-oscillatory high order calculations (Burguete and García-Navarro, 2001), unsteady boundary conditions

(Burguete et al., 2006), solute transport (Burguete et al., 2007a) and dominant friction terms (Burguete et al., 2007b, 2008). In order to extend those developments to furrow irrigation simulation, specific models have been adapted to formulate friction, solute dispersion, infiltration and junctions in furrows and furrow networks (Burguete et al., 2009a,b).

The objective of the present work is the development of a software tool to simulate the complete water flow dynamics and solute transport in furrows and furrow networks with a basis on the exhaustive verification and validation performed in Burguete et al. (2009a,b). The software *surcos* has been designed to incorporate the cited modelling improvements in a user friendly, reliable, robust and efficient tool.

First, the governing equations used are outlined in order to state the notation. Second, the numerical scheme used in the simulation engine is detailed to enable an easy reproduction of the model. Then, the main components of the software interface are presented. Finally, some examples of use are included to illustrate the performance.

The model and the examples presented in this work are distributed (Burguete et al., 2013a,b) as free software under a Berkeley Software Distribution (BSD) type license with available and editable source code.

2. Physical model

2.1. Shallow-water model

The one-dimensional system formed by the cross sectional averaged liquid and solute mass conservation, momentum balance in main stream direction, infiltration and solute transport in prismatic open channels can be expressed in conservative form as (Burguete et al., 2009a):

$$\frac{\partial \vec{U}}{\partial t} + \frac{\partial \vec{F}}{\partial l} = \vec{I} + \vec{S}^c + \frac{\partial \vec{D}}{\partial l}, \tag{1}$$

where $\vec{U}$ is the vector of conserved variables, t is the time, $\vec{F}$ the flux vector, l the longitudinal coordinate, $\vec{I}$ the infiltration vector, $\vec{S}^c$ the source term vector, and $\vec{D}$ stands for solute dispersion:

$$\vec{U} = \begin{pmatrix} A \\ Q \\ A\,s \end{pmatrix}, \quad \vec{F} = \begin{pmatrix} Q \\ g\,I_1 + \frac{Q^2}{A} \\ Q\,s \end{pmatrix}, \quad \vec{S}^c = \begin{pmatrix} 0 \\ g\,A\,(S_0 - S_f) \\ 0 \end{pmatrix},$$

$$\vec{I} = \begin{pmatrix} -P\,I \\ 0 \\ -P\,I\,s \end{pmatrix}, \quad \vec{D} = \begin{pmatrix} 0 \\ 0 \\ K_l\,A\frac{\partial s}{\partial l} \end{pmatrix}, \qquad (2)$$

with A the wetted cross sectional area, Q the discharge, s the cross sectional average solute concentration, g the gravity acceleration, S_0 the longitudinal bottom slope, S_f the longitudinal friction slope, K_l the longitudinal solute dispersion coefficient, I the infiltration rate, P the cross-sectional wetted perimeter and I_1 represents pressure forces.

The furrows are modeled as pervious prismatic channels of trapezoidal cross section as represented in Figure 1. In this case, the pressure integral becomes (Burguete et al., 2009a):

$$I_1 = \frac{B_0\,h^2}{2} + \frac{Z\,h^3}{3}, \qquad (3)$$

The set of equations is completed with the laws for infiltrated volume of water and solute (Burguete et al., 2009a):

$$\frac{\partial \alpha}{\partial t} = P\,I, \quad \frac{\partial \phi}{\partial t} = P\,I\,s, \qquad (4)$$

with α the volume of water infiltrated per unit length of furrow and ϕ the mass of solute infiltrated per unit length of the furrow.

The Jacobian matrix of the flow can be expressed as (Burguete et al., 2009a):

$$\mathbf{J} = \frac{\partial \vec{F}}{\partial \vec{U}} = \begin{pmatrix} 0 & 1 & 0 \\ c^2 - u^2 & 2u & 0 \\ -u\,s & s & u \end{pmatrix}, \qquad (5)$$

where $u = \frac{Q}{A}$ is the cross sectional average velocity, $c = \sqrt{\frac{g\,A}{B}}$ is the velocity of the infinitesimal waves and B is the cross section top width. This matrix can

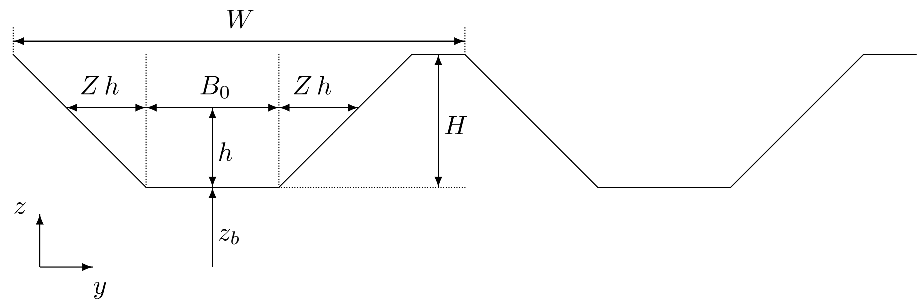

Figure 1: Trapezoidal furrow geometry. h is the water depth, W the distance between furrows, z_b the bottom level, H the furrow depth, B_0 the base width and Z the tangent of the angle between the furrow walls and the vertical direction.

be made diagonal (Burguete et al., 2009a):

$$\mathbf{J} = \mathbf{P}\,\mathbf{\Lambda}\,\mathbf{P}^{-1}, \quad \mathbf{P} = \begin{pmatrix} 1 & 1 & 0 \\ \lambda^1 & \lambda^2 & 0 \\ s & s & 1 \end{pmatrix}, \quad \mathbf{\Lambda} = \begin{pmatrix} \lambda^1 & 0 & 0 \\ 0 & \lambda^2 & 0 \\ 0 & 0 & \lambda^3 \end{pmatrix}, \tag{6}$$

with $\mathbf{\Lambda}$ the eigenvalues diagonal matrix, $\mathbf{P}$ the diagonalizer matrix and λ^k the Jacobian eigenvalues corresponding to the propagation characteristic celerities:

$$\lambda^1 = u + c, \quad \lambda^2 = u - c, \quad \lambda^3 = u. \tag{7}$$

2.2. Furrow infiltration model

The infiltration rate is calculated using the Kostiakov-Lewis model modified by Burguete et al. (2009a) in furrows:

$$I = I_c + K\,a \left(\frac{\alpha}{K\,W}\right)^{\frac{a-1}{a}}, \tag{8}$$

where K is the Kostiakov constant and a is the Kostiakov exponent, both empirical parameters depend on soil type, soil water and compaction, and I_c is the saturated infiltration long-term rate (Walker and Skogerboe, 1987).

2.3. Friction model

The friction slope can be modeled by means of the Gauckler-Manning law (Gauckler, 1867; Manning, 1890) that, for a furrow of trapezoidal cross section is (Burguete et al., 2009a):

$$S_f = \frac{n^2\, Q\, |Q| \left(B_0 + 2\, h\, \sqrt{1 + Z^2}\right)^{4/3}}{\left(B_0\, h + Z\, h^2\right)^{10/3}}. \tag{9}$$

The program *surcos* can calculate the friction with the model proposed in Burguete et al. (2007b, 2008), that in furrows with trapezoidal cross section is (Burguete et al., 2009a):

$$S_f = \frac{\epsilon\, (b+1)^2\, d^{2\,b}\, |Q|\, Q}{g \left\{ B_0 \left(h^{b+\frac{3}{2}} - \sqrt{h}\, d^{1+b} \right) + 2\, Z \left[\frac{h^{b+\frac{5}{2}} - d^{b+\frac{5}{2}}}{b+\frac{5}{2}} - \frac{2}{3} d^{1+b} \left(h^{\frac{3}{2}} - d^{\frac{3}{2}} \right) \right] \right\}^2}, \tag{10}$$

where b is a fitting exponent of the vertical profile of flow velocity, d is a characteristic length of the bed roughness irregularities, ϵ is a dimensionless parameter of aerodynamical resistance depending only, in turbulent flows, on the roughness shape. In furrows, $b = 0.27$ is used based in rivers measurements (Burguete et al., 2007b). This friction law is only valid for $h > d$. If $h < d$ a zero velocity condition ($Q = 0$) is imposed.

2.4. Solute dispersion model

The diffusion coefficient contains all the information related to molecular or viscous diffusion, turbulent diffusion and dispersion derived from the averaging process. A model suggested in Rutherford (1994) will be used for practical applications:

$$K_l = 10\, \sqrt{g\, P\, A\, |S_f|}. \tag{11}$$

3. Numerical model

3.1. Mesh

In every furrow, the discrete mesh longitudinal coordinates are defined as:

$$l_i = \frac{i-1}{N-1}\, L, \tag{12}$$

with l_i the longitudinal coordinate, N the number of cells discretizing the furrow and L the furrow length. The size of every cell δl_i and the distance between

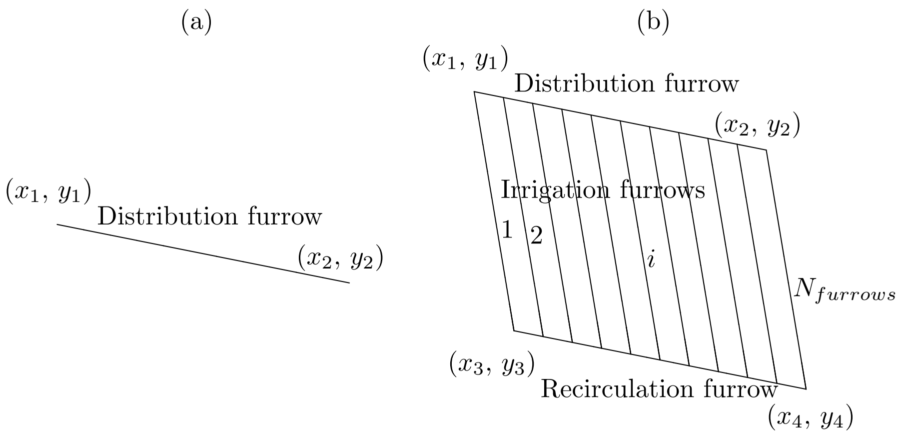

Figure 2: Possible geometry configurations in *surcos*: (a) isolated furrow ($N_{furrows} = 0$), where only the distribution furrow is simulated, (b) furrow irrigation network ($N_{furrows} > 0$). The recirculation furrow is optional.

cells $\delta l_{i+(1/2)}$ is defined as:

$$\delta l_{i+(1/2)} = l_{i+1} - l_i = \frac{L}{N-1},$$

$$\delta l_i = \frac{L}{N-1}, \ (i < N \text{ and } i > 1), \quad \delta l_1 = \delta l_N = \frac{1}{2}\frac{L}{N-1}. \tag{13}$$

The program *surcos* can only be used for furrows of uniform slope. The grid cells bed level is computed by interpolation from the furrows end points.

3.2. Sub-steps

The numerical scheme used in this paper is based on a seven sub-steps algorithm very similar to the proposed in Burguete et al. (2009a):

1. In the first sub-step, the flow equations and the advective part of the transport equation are discretized with the explicit scheme:

$$\vec{U}_i^a = \vec{U}_i^n + \Delta t^n \left(\vec{S}^c - \frac{\partial \vec{F}}{\partial l} \right)_i^n. \tag{14}$$

2. In a second sub-step the solute diffusion term is discretized implicitly:

$$\vec{U}_i^b = \vec{U}_i^a + \Delta t^n \left(\frac{\partial \vec{D}}{\partial l} \right)_i^b. \tag{15}$$

3. In a third sub-step infiltration is discretized as follows:

$$\vec{U}_i^c = \vec{U}_i^b + \Delta t^n \, \vec{I}_i^c. \tag{16}$$

4. In a fourth sub-step, the source terms are added with an implicit discretization:

$$\vec{U}_i^d = \vec{U}_i^c + \theta \, \Delta t^n \left(\vec{S}_i^d - \vec{S}_i^c \right). \tag{17}$$

   where $\theta = 0.5$ is the parameter controlling the degree of implicitness of the source term.

5. In a fifth sub-step, the boundary conditions are applied at the inlet, outlet and external mass sources $\vec{U}_i^e$.

6. In a sixth sub-step, the furrow confluences (characteristic of level furrow networks) are computed to obtain $\vec{U}_i^f$.

7. Finally, the solute solubility is considered to obtain the conserved variables $\vec{U}_i^{n+1}$ at the next time step.

3.3. First sub-step: surface flow and transport

This sub-step is limitant for the time step size compatible with the numerical stability of the schemes used in the present code (Burguete et al., 2009a). The time step size is selected according to:

$$\Delta t^n = t^{n+1} - t^n = \mathrm{CFL} \, \min_i \left(\frac{\min \left(\delta l_{i+(1/2)}, \, \delta l_{i-(1/2)} \right)}{\max_k \left(\left| \lambda_i^k \right| \right)} \right), \tag{18}$$

with CFL the dimensionless Courant-Friedrichs-Lewy number (Courant et al., 1928).

A numerical limitation of the friction source term is performed in order to avoid non-physical friction forces (Burguete et al., 2008):

$$\left(g \, A \, S_f \, \delta l \right)_{i+(1/2)}^n = \min \left[\frac{\left(g \, A \, S_f \right)_{i+1}^n + \left(g \, A \, S_f \right)_i^n}{2} \, \delta l_{i+(1/2)}, \right.$$
$$\left. \frac{\left(Q \, \delta l \right)_{i+(1/2)}^n}{\Delta t^n} - \delta \left(\frac{Q^2}{A} \right)_{i+(1/2)}^n - \left(g \, \delta I_1 \right)_{i+(1/2)}^n \right], \tag{19}$$

where the notation $\delta f_{i+(1/2)} = f_{i+1} - f_i$ and $f_{i+(1/2)} = (f_{i+1} + f_i)/2$ has been used. Defining the Jacobian eigenvalues with the Roe's (Roe, 1981; Burguete et al., 2009a) averages:

$$\overline{\lambda}_{i+(1/2)} = \frac{\sqrt{A_{i+1}}\,\lambda_{i+1} + \sqrt{A_i}\,\lambda_i}{\sqrt{A_{i+1}} + \sqrt{A_i}}, \quad \overline{s}_{i+(1/2)} = \frac{\sqrt{A_{i+1}}\,s_{i+1} + \sqrt{A_i}\,s_i}{\sqrt{A_{i+1}} + \sqrt{A_i}}. \tag{20}$$

Then, defining the first order upwind coefficients as:

$$\delta F = -g\,A\,(\delta z_b + S_f\,\delta l) - \delta\left(\frac{Q^2}{A} + g\,\delta I_1\right), \quad o_k^{\pm} = \frac{1}{2}\left[1 \pm \mathrm{sign}\left(\overline{\lambda}^k\right)\right],$$

$$\delta w_1 = \frac{-\overline{\lambda}^2\,\delta Q + \delta F}{\overline{\lambda}^1 - \overline{\lambda}^2}, \quad \delta w_2 = \frac{\overline{\lambda}^1\,\delta Q - \delta F}{\overline{\lambda}^1 - \overline{\lambda}^2}, \quad \delta w_3 = \delta\,(Q\,s) - \overline{s}\,\delta Q,$$

$$G_1^{\pm} = o_1^{\pm}\,\delta w_1 + o_2^{\pm}\,\delta w_2, \quad G_2^{\pm} = o_1^{\pm}\,\overline{\lambda}^1\,\delta w_1 + o_2^{\pm}\,\overline{\lambda}^2\,\delta w_2, \quad G_3^{\pm} = \overline{s}\,G_1^{\pm} + \delta w_3, \tag{21}$$

the high order TVD coefficients as:

$$\psi(r) = \max[0,\ \min(2,\ r),\ \min(r,\ 2\,r)],$$

$$L_1^{\pm} = \frac{1}{2}\left(1 \mp \frac{\Delta t}{\delta l}\,o_1^{\pm}\overline{\lambda}^1\right)\frac{-\overline{\lambda}^2\,G_1^{\pm} + G_2^{\pm}}{\overline{\lambda}^1 - \overline{\lambda}^2},$$

$$L_2^{\pm} = \frac{1}{2}\left(1 \mp \frac{\Delta t}{\delta l}\,o_2^{\pm}\overline{\lambda}^2\right)\frac{\overline{\lambda}^1\,G_1^{\pm} - G_2^{\pm}}{\overline{\lambda}^1 - \overline{\lambda}^2},$$

$$L_3^{\pm} = \frac{1}{2}\left(1 \mp \frac{\Delta t}{\delta l}\,o_3^{\pm}\overline{\lambda}^3\right)\left(G_3^{\pm} - \overline{s}\,G_1^{\pm}\right),$$

$$\left(\Psi_k^{\pm}\right)_{i+(1/2)} = \psi\left(\frac{\left(L_k^{\pm}\right)_{i+(1/2)\pm1}}{\left(L_k^{\pm}\right)_{i+(1/2)}}\right), \quad R_1^{\pm} = \Psi_1^{\pm}\,L_1^{\pm} + \Psi_2^{\pm}\,L_2^{\pm},$$

$$R_2^{\pm} = \overline{\lambda}^1\,\Psi_1^{\pm}\,L_1^{\pm} + \overline{\lambda}^2\,\Psi_2^{\pm}\,L_2^{\pm}, \quad R_3^{\pm} = \overline{s}\,R_1^{\pm} + \Psi_3^{\pm}\,L_3^{\pm}, \tag{22}$$

and the artificial viscosity coefficient as in Burguete and García-Navarro (2004):

$$\nu_{i+(1/2)}^n = \max_k \begin{cases} \frac{1}{4}\left[\delta(\lambda^k) - 2\left|\overline{\lambda}^k\right|\right]_{i+(1/2)}, & \text{if } (\lambda^k)_i^n < 0 \text{ and } (\lambda^k)_{i+1}^n > 0; \\ 0, & \text{otherwise;} \end{cases} \tag{23}$$

the second order in space and time TVD scheme (Burguete et al., 2007a) can be written as:

$$
\begin{pmatrix} A \\ Q \\ A\,s \end{pmatrix}_i^a = \begin{pmatrix} A \\ Q \\ A\,s \end{pmatrix}_i^n + \frac{\Delta t^n}{\delta l_i} \left[- \begin{pmatrix} R_1^+ \\ R_2^+ \\ R_3^+ \end{pmatrix}_{i-(3/2)}^n - \begin{pmatrix} R_1^- \\ R_2^- \\ R_3^- \end{pmatrix}_{i+(3/2)}^n \right.
$$

$$
\left. + \begin{pmatrix} G_1^+ + R_1^+ - \nu\,\delta A \\ G_2^+ + R_2^+ - \nu\,\delta Q \\ G_3^+ + R_3^+ - \nu\,\delta(A\,s) \end{pmatrix}_{i-(1/2)}^n + \begin{pmatrix} G_1^- + R_1^- + \nu\,\delta A \\ G_2^- + R_2^- + \nu\,\delta Q \\ G_3^- + R_3^- + \nu\,\delta(A\,s) \end{pmatrix}_{i+(1/2)}^n \right], \tag{24}
$$

and, at the boundary points:

$$
\begin{pmatrix} A \\ Q \\ A\,s \end{pmatrix}_1^a = \begin{pmatrix} A \\ Q \\ A\,s \end{pmatrix}_1^n + \frac{\Delta t^n}{\delta l_1} \left[- \begin{pmatrix} R_1^- \\ R_2^- \\ R_3^- \end{pmatrix}_{5/2}^n \right.
$$

$$
\left. + \begin{pmatrix} G_1^- + R_1^- + \nu\,\delta A \\ G_2^- + R_2^- + \nu\,\delta Q \\ G_3^- + R_3^- + \nu\,\delta(A\,s) \end{pmatrix}_{3/2}^n \right],
$$

$$
\begin{pmatrix} A \\ Q \\ A\,s \end{pmatrix}_2^a = \begin{pmatrix} A \\ Q \\ A\,s \end{pmatrix}_2^n + \frac{\Delta t^n}{\delta l_2} \left[- \begin{pmatrix} R_1^- \\ R_2^- \\ R_3^- \end{pmatrix}_{7/2}^n \right.
$$

$$
\left. + \begin{pmatrix} G_1^+ + R_1^+ - \nu\,\delta A \\ G_2^+ + R_2^+ - \nu\,\delta Q \\ G_3^+ + R_3^+ - \nu\,\delta(A\,s) \end{pmatrix}_{3/2}^n + \begin{pmatrix} G_1^- + R_1^- + \nu\,\delta A \\ G_2^- + R_2^- + \nu\,\delta Q \\ G_3^- + R_3^- + \nu\,\delta(A\,s) \end{pmatrix}_{5/2}^n \right],
$$

$$
\begin{pmatrix} A \\ Q \\ A\,s \end{pmatrix}_{N-1}^a = \begin{pmatrix} A \\ Q \\ A\,s \end{pmatrix}_{N-1}^n + \frac{\Delta t^n}{\delta l_{N-1}} \left[- \begin{pmatrix} R_1^+ \\ R_2^+ \\ R_3^+ \end{pmatrix}_{N-(5/2)}^n \right.
$$

$$
\left. + \begin{pmatrix} G_1^+ + R_1^+ - \nu\,\delta A \\ G_2^+ + R_2^+ - \nu\,\delta Q \\ G_3^+ + R_3^+ - \nu\,\delta(A\,s) \end{pmatrix}_{N-(3/2)}^n + \begin{pmatrix} G_1^- + R_1^- + \nu\,\delta A \\ G_2^- + R_2^- + \nu\,\delta Q \\ G_3^- + R_3^- + \nu\,\delta(A\,s) \end{pmatrix}_{N-(1/2)}^n \right],
$$

$$
\begin{pmatrix} A \\ Q \\ A\,s \end{pmatrix}_N^a = \begin{pmatrix} A \\ Q \\ A\,s \end{pmatrix}_N^n + \frac{\Delta t^n}{\delta l_N} \left[- \begin{pmatrix} R_1^+ \\ R_2^+ \\ R_3^+ \end{pmatrix}_{N-(3/2)}^n + \begin{pmatrix} G_1^+ + R_1^+ - \nu\,\delta A \\ G_2^+ + R_2^+ - \nu\,\delta Q \\ G_3^+ + R_3^+ - \nu\,\delta(A\,s) \end{pmatrix}_{N-(1/2)}^n \right]. \tag{25}
$$

3.4. Second sub-step: solute dispersion

Defining:

$$
(K_l\,A)_{i+(1/2)} = \min\left[(K_l\,A)_i\,,\ (K_l\,A)_{i+1}\right], \tag{26}
$$

the following Eulerian implicit centered scheme is used to solve the surface flow solute dispersion:

$$
\begin{aligned}
&\left[\delta l_1\,A_1^b + \left(\frac{K_l\,A\,\Delta t^n}{\delta l}\right)_{3/2}^b\right] s_1^b - \left(\frac{K_l\,A\,\Delta t^n}{\delta l}\right)_{3/2}^b s_2^b = \delta l_1\,A_1^a\,s_1^a,\\
&-\left(\frac{K_l\,A\,\Delta t^n}{\delta l}\right)_{i-(1/2)}^b s_{i-1}^b\\
&+\left[\delta l_i\,A_i^b + \left(\frac{K_l\,A\,\Delta t^n}{\delta l}\right)_{i-(1/2)}^b + \left(\frac{K_l\,A\,\Delta t^n}{\delta l}\right)_{i+(1/2)}^b\right] s_i^b\\
&-\left(\frac{K_l\,A\,\Delta t^n}{\delta l}\right)_{i+(1/2)}^b s_{i+1}^b = \delta l_i\,A_i^a\,s_i^a,\\
&-\left(\frac{K_l\,A\,\Delta t^n}{\delta l}\right)_{N-(1/2)}^b s_{N-1}^b + \left[\delta l_N\,A_N^b + \left(\frac{K_l\,A\,\Delta t^n}{\delta l}\right)_{N-(1/2)}^b\right] s_N^b\\
&= \delta l_N\,A_N^a\,s_N^a,
\end{aligned} \tag{27}
$$

being a tridiagonal system of N equations with N variables (s_i^b) at every furrow solved with a Gaussian elimination algorithm.

3.5. Third sub-step: infiltration

In a third step, the contribution of the infiltration term is incorporated as in Burguete et al. (2009a):

$$
\begin{aligned}
&\Delta\alpha_i^b = \min(A,\ \Delta t^n\,P\,I)_i^b, \quad A_i^c = A_i^b - \Delta\alpha_i^b, \quad A_i^c\,s_i^c = \left(A_i^b - \Delta\alpha_i^b\right) s_i^b,\\
&\alpha_i^c = \alpha_i^b + \Delta\alpha_i^b, \quad \phi_i^c = \phi_i^b + \Delta\alpha_i^b\,s_i^b.
\end{aligned} \tag{28}
$$

3.6. Fourth sub-step: source terms

In the fourth sub-step an implicit discretization of the source terms is applied. Taking into account that only the momentum equation contains source terms, the mass conservation and the solute transport equations are trivial in this step :

$$A_i^d = A_i^c, \quad (A\,s)_i^d = (A\,s)_i^c. \tag{29}$$

The friction laws considered are singular, tending to infinity for small values of the water depth, which can introduce numerical instabilities in transient calculations. A threshold value for the depth h_{min} will be used in order to avoid those situations. Below that value, the discharge will be set to zero. We use:

- $h_{min} = 0.01$ m for the Manning friction model.
- $h_{min} = d$ for the power law velocity model.

otherwise, a friction factor $r = r(A) = \frac{S_f}{|Q|\,Q}$ depending only of A is defined for the considered friction models, leading to a simple second order equation for the water discharge. Therefore, discharge is evaluated according to:

$$Q_i^d = \left\{ \begin{array}{ll} 0, & \left(h_i^d \le h_{min}\right); \\ Q_i^c + g\,\theta\,\Delta t^n \left\{ [A\;(S_0 - r\,|Q|\,Q)]_i^d \right. & \\ \left. \qquad - [A\;(S_0 - r\,|Q|\,Q)]_i^c \right\}, & \left(h_i^d > h_{min}\right); \end{array} \right. \tag{30}$$

3.7. Fifth step: boundary conditions

3.7.1. Inlet and outlet

The program *surcos* always assumes the the furrows are closed at both ends. This is achieved by means of:

$$Q_1^e = Q_N^e = 0. \tag{31}$$

3.7.2. Mass sources

All the mass inflows, both of water or solute, are treated in *surcos* as internal source points. A water inflow point at the location $\vec{r}_{in}$ with a discharge $Q_{in}(t)$ is dealt with by searching the nearest i-th grid cell where the following is assigned:

$$A_i^e = A_i^d + \frac{1}{\delta l_i} \int_{t^n}^{t^{n+1}} Q_{in}(t)\, dt; \tag{32}$$

or, in case of having a solute inflow point:

$$(A\, s)_i^e = (A\, s)_i^d + \frac{1}{\delta l_i} \int_{t^n}^{t^{n+1}} Q_{in}(t)\, dt. \tag{33}$$

In the rest of the grid cells nothing is altered:

$$\vec{U}_i^e = \vec{U}_i^d. \tag{34}$$

3.8. Sixth sub-step: furrow junctions

We will concentrate on furrow junctions of the "T" type, that is, involving only a main furrow and a perpendicular secondary furrow. In this way, the momentum addition from the tributary furrow is in the normal direction to the main flow and viceversa.

The main hypothesis used to solve at the junction area is that the main furrow grid cell involved at the junction (j) as well as the secondary furrow grid cell involved (k) share a unique water surface level and a unique value of solute concentration. The total volume of water $V_{junction}^e$ and mass of solute $M_{junction}^e$ at the junction cells are therefore (Burguete et al., 2009a):

$$V_{junction}^e = A_k^e\, \delta l_k + A_j^e\, \delta l_j, \quad M_{junction}^e = (A\, s)_k^e\, \delta l_k + (A\, s)_j^e\, \delta l_j. \tag{35}$$

By requiring the conservation of water volume and the uniform surface water level z_s^f, a second order equation for this variable can be written in a trapezoidal furrow geometry:

$$\begin{aligned} &\left[B_0 + Z\, \left(z_s^f - z_b\right)\right]_k\, \left(z_s^f - z_b\right)_k\, \delta l_k + \left[B_0 + Z\, \left(z_s^f - z_b\right)\right]_j\, \left(z_s^f - z_b\right)_j\, \delta l_j \\ &= V_{junction}^e. \end{aligned} \tag{36}$$

This formulation immediately leads to the values of A_i^f and A_k^f. On the other hand, the requirements of solute mass conservation and uniform concentration at the junction result in:

$$s_j^f = s_k^f = \frac{M_{junction}^e}{V_{junction}^e}. \tag{37}$$

The rest of the grid points not involved in the junction are not altered in the present sub-step:

$$\vec{U}_i^f = \vec{U}_i^e. \tag{38}$$

3.9. Final sub-step: solute solubility

Finally, the fertilizer instantaneous solubility S is considered. No dissolution velocity is assumed. Defining m_i as the solid mass deposed at cell i, the following is performed:

$$S \geq s_i^f \text{ and } m_i^n = 0 \;\Rightarrow\; s_i^{n+1} = s_i^f, \quad m_i^{n+1} = 0;$$

$$S \geq s_i^f \text{ and } m_i^n \leq \left(S - s_i^f\right) A_i^f\, \delta l_i \;\Rightarrow\; s_i^{n+1} = s_i^f + \frac{m_i^n}{A_i^f\, \delta l_i}, \quad m_i^{n+1} = 0;$$

$$S \geq s_i^f \text{ and } m_i^n > \left(S - s_i^f\right) A_i^f\, \delta l_i \;\Rightarrow\; s_i^{n+1} = S,$$

$$m_i^{n+1} = m_i^n - \left(S - s_i^f\right) A_i^f\, \delta l_i;$$

$$S < s_i^f \;\Rightarrow\; s_i^{n+1} = S, \quad m_i^{n+1} = m_i^n + \left(s_i^f - S\right) A_i^f\, \delta l_i. \tag{39}$$

The solubility only affects the solute concentration. The rest of the variables remain unchanged:

$$A_i^{n+1} = A_i^f, \quad Q_i^{n+1} = Q_i^f. \tag{40}$$

4. Interface

This section describes the windows interface in *surcos*. The simulation engine has been coded in standard C-language. The graphical interface has also been coded in C-language using some multiplatform free libraries:

Gettext: to support different international languages. Currently english, spanish, french and italian versions are available.

GTK+: to show the interactive windows.

OpenGL / FreeGLUT: to display the graphical results.

Libpng: to save the graphical plots.

The program has been tested in multiple operative systems: Windows XP[1], Windows 7[1], Debian Linux, FreeBSD, OpenBSD, NetBSD, DragonflyBSD and OpenIndiana.

4.1. Main window

The main window appears when launching the program and is used as basic interface with the user. It contains the links to get access to the rest of the windows. Using the buttons in table 1 it is possible to get access to the different utilities in the program.

Figure 3: Initial and main window in the application *surcos*.

Table 1: Description of the different actions offered by the main menu *surcos*.

Button	Role
Open	Open a window to load a project
Configure	Open a window to configure the project
Execute	Run the simulation
Plot	Open a window for results visualization
Summary	Open a summary window
Help	Information
Quit	Exit the application

4.2. Configuration window

The window to configure a simulation can be accessed by pressing on the button *Configure*. Some panels can be accessed in this window.

4.2.1. Geometry configuration panel

Program *surcos* simulates irrigation in a quadrilateral network of furrows or in a isolated furrow. The geometry configuration panel (see figure 4), can be used to edit the project topographic data by means of the coordinates of the four vertices that define the furrow plot.

[1]Windows XP and Windows 7 are trademarks of Microsoft Corporation.

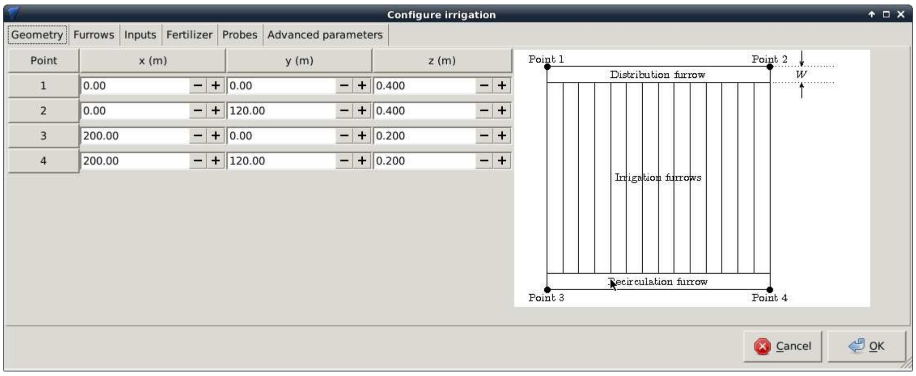

Figure 4: Geometry configuration panel.

As displayed in figure 4, the distribution furrow runs between points 1 and 2 and the recirculation furrow, if any, can be defined between points 3 and 4. The irrigation furrows are assumed in the normal direction to the former. In cases of isolated furrow only the distribution furrow between points 1 and 2 is simulated.

4.2.2. Furrow configuration panel

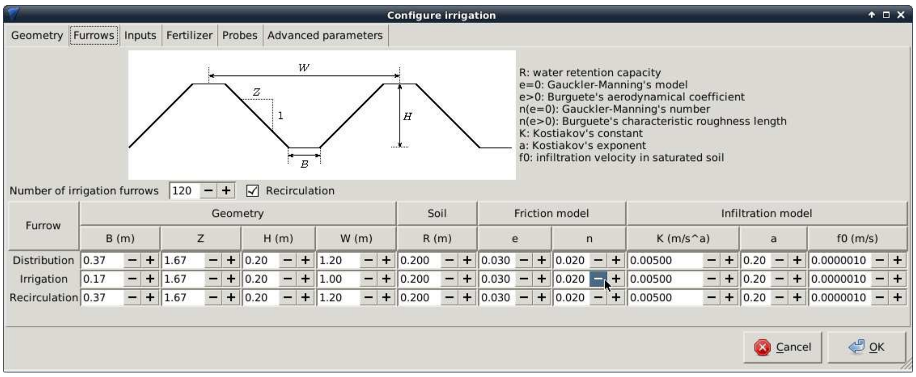

Figure 5: Furrow configuration panel.

The panel displayed in figure 5 allows to define the geometric properties of the furrows as divided in three types: distribution, recirculation and irrigation furrows. The different options appear as active or inactive depending on the previous definition of the furrow in our project. The available characteristics to edit are all displayed in figure 5. In cases of isolated furrow simulations the number of irrigation furrows must be set to 0 and the furrow characteristics must be set at the distribution furrow.

4.2.3. Inlet configuration panel

The panel shown in figure 6 can be used to configure the total water and fertilizer inlet to the furrow system. Every inlet is assigned to a location point where the flow is applied, and is characterized by the initial and the final application times of a constant discharge. Note that, if the point assigned falls out of a furrow, the program finds the nearest position within a furrow. The discharge is volumetric rate flow for the water and a mass flow rate for the fertilizer. It is possible to define more complex inlet hydrographs by means of a sequence of inlet discharges at the same point.

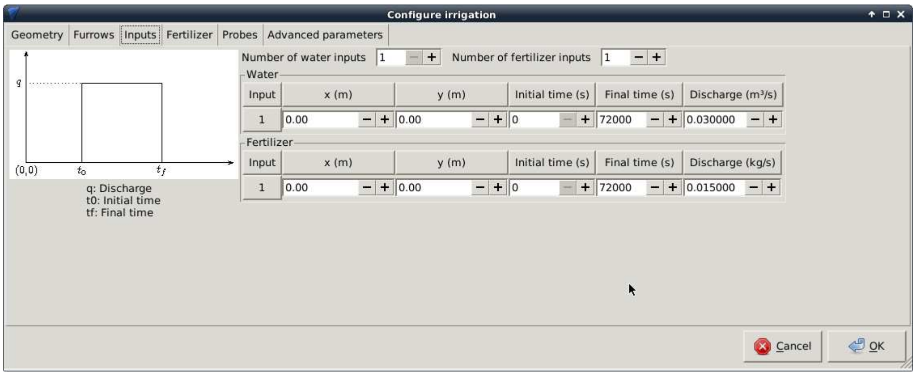

Figure 6: Inlet configuration panel.

4.2.4. Fertilizer configuration panel

The solubility characteristics of the fertilizer can be set too.

4.2.5. Probes configuration panel

The panel displayed in figure 7 can be used to define the number of probes and their location in the plot. Note that, if the point assigned falls out of a furrow, the program finds the nearest position within a furrow.

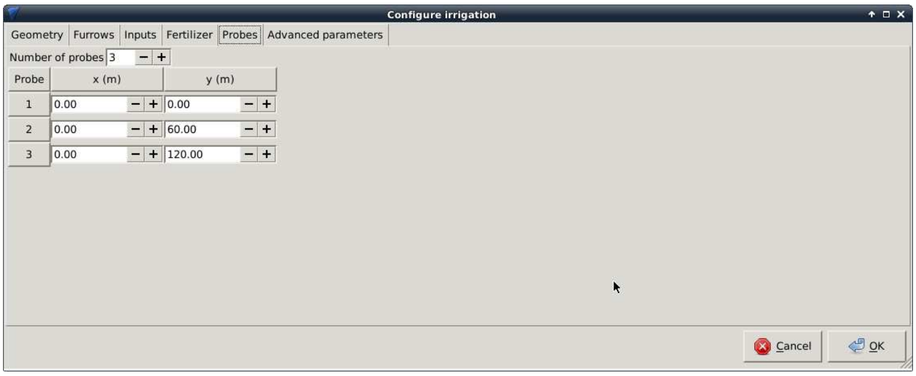

Figure 7: Probes configuration panel.

4.2.6. Advanced parameters configuration panel

The panel shown in figure 8 contains advanced options to configure the numerical simulation, as follow:

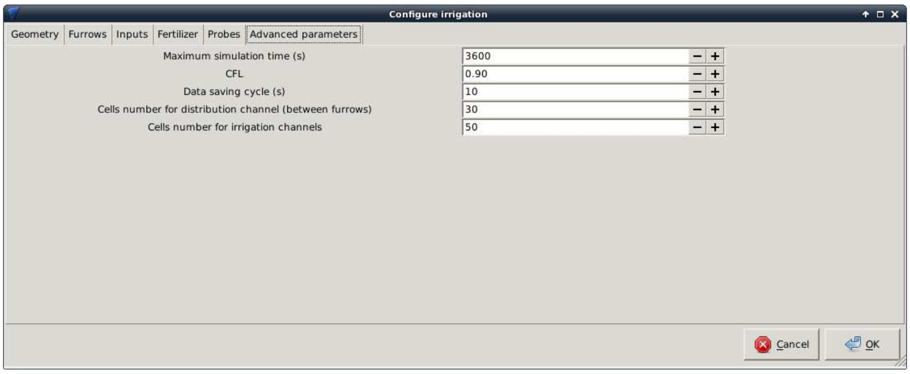

Figure 8: Advanced parameters configuration panel.

Maximum simulation time: Usually, *surcos* runs the simulation from the initial conditions up to the moment all the applied water has infiltrated in the terrain. In order to avoid excessively long simulation times, this parameter can be used to state a horizon or target time. From that limit, the computation stops even though some water still remains on the surface.

CFL: Dimensionless numerical parameter proportional to the time step size used by the resolution method. It takes values between 0 and 1 for numerical stability reasons. Values close to 1 are optimal. Excessively low values can slow the computation.

Data saving cycle: Simulation time interval used to save series of numerical results in a file. It is possible to have $n = \frac{t_s}{p_v}$ snapshots of the irrigation event, with t_s the simulation time and p_v the data saving cycle.

Cells number for distribution furrow (between irrigation furrows): Number of computational cells in the distribution/recirculation furrow between two irrigation furrows. A diagram can be shown in figure 9. In cases of isolated furrow this is the number of cells of the mesh.

Cells number for irrigation furrows: Number of computational cells in every irrigation furrow. See an example in figure 9. More cells implies better quality in the results and slower computations.

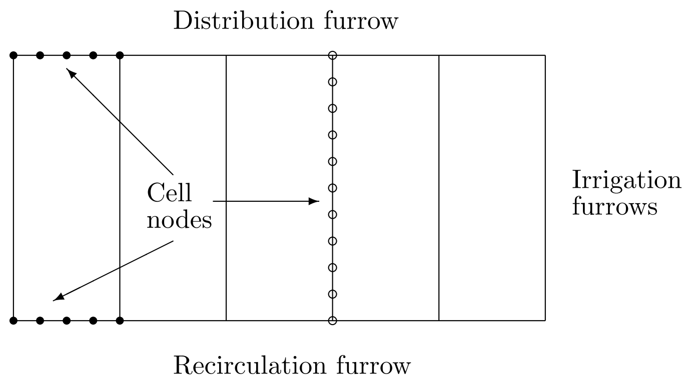

Figure 9: Mesh example on a furrow network. This example has 6 irrigation furrows, 5 cells at the distribution furrow between irrigation furrows (•) and 11 cells at every irrigation furrow (○).

4.3. Simulation

After the configuration, the simulation of the project is performed by pressing the button *Execute* in the main menu.

4.4. Results visualization

4.4.1. Graphical results

A window showing a graphical plot of the numerical results can be accessed by pressing the button *Plot*. The graphics are controlled from the window shown in figure 10, where an interactive dial can be used to move forward and backward in time the evolution of the variables represented. It is also possible to choose the furrow, the variable and the probe to view. The program offers the possibility to save the graphical results by pressing the button *Save* at the bottom of the window. The image of the plot appearing on the graphical window in that moment, as the shown in next section in figures 15-17, is saved in a *png* format.

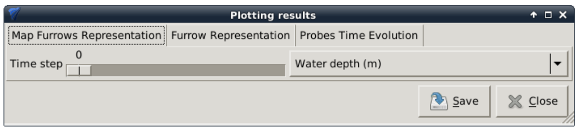

Figure 10: Plot selection window

Program *surcos* produces three types of plots. The first is a plan view of the furrow network, with the possibility to display the distribution in the network. The second graphical option is a Cartesian *xy*-plot of the longitudinal profile along different furrows. The third graphical option is a time evolution of the variables in the different probes. The variables that can be plotted are those in table 2.

Some examples of these graphics provided by the program are shown in the next section (figures 15-17).

4.4.2. Summary

The access to the summary is through the button *Summary*. This is useful to produce a brief text report with the description of the irrigation configuration and the most relevant results obtained. An example is displayed in figure 11.

The results include the surface, infiltrated and percolated water and fertilizer mass both in the irrigation furrows and in the distribution/recirculation furrows.

Table 2: Variables to view on the plots.

Variable	Units	Furrows network	Furrow profile	Probe evolution
Surface water depth	m	x	x	x
Surface fertilizer concentration	kg m^{-3}	x	x	x
Infiltrated water volume per unit furrow length	m^2	x	x	-
Infiltrated fertilizer mass per unit furrow length	kg m^{-1}	x	x	-
Discharge	m^3 s^{-1}	-	x	-
Surface water volume per unit furrow length	m^2	-	x	-
Surface fertilizer mass per unit furrow length	kg m^{-1}	-	x	-
Surface water and bed levels	m	-	x	-
Irrigation advance and recession times	s	-	x	-

The infiltrated water mass in the soil remains available to the crops by retention forces, contrary to the percolated water.

The uniformity of distribution of water (UW_{25}) and of the fertilizer (UF_{25}) follows the ratio between the infiltration average of the 25% of the less irrigated points and the total infiltration average:

$$UW_{25} = \frac{\displaystyle\sum_{\alpha_i < 25\%} \min\left(\alpha_i,\, R_i\, W\right)}{\displaystyle\sum_i \min\left(\alpha_i,\, R_i\, W\right)}, \quad UF_{25} = \frac{\displaystyle\sum_{\phi_i < 25\%} \min\left(\phi_i,\, \frac{R_i\, W\, \phi_i}{\alpha_i}\right)}{\displaystyle\sum_i \min\left(\phi_i,\, \frac{R_i\, W\, \phi_i}{\alpha_i}\right)}, \tag{41}$$

with R the water retention capacity of the soil. In furrow networks the uniformity of distribution is calculated only in the irrigation furrows.

Finally, the efficiency is computed as the infiltrated mass in the irrigation furrows divided by the total applied mass. Therefore, both the percolated mass and the solid mass of solute, as well as the mass infiltrated in the distribution/recirculation furrows in cases of furrow networks, are considered losses in the estimation of the efficiency.

5. Results

This section is devoted to the presentation of examples of the numerical results produced by the model in several scenarios of fertigation in furrows

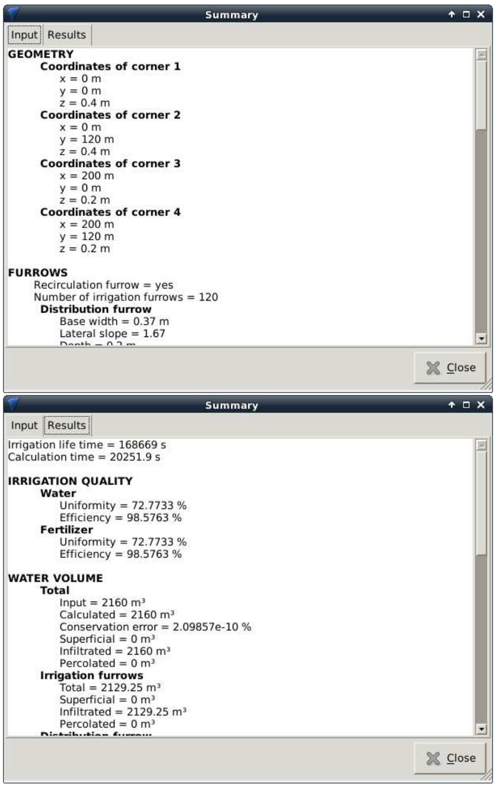

Figure 11: Summary of the input data (top) and results (bottom).

and furrow networks. All the necessary input files for these examples can be downloaded from Burguete et al. (2013a) or Burguete et al. (2013b).

5.1. Simulation of 9 fertigation scenarios in a level isolated furrow

A single zero slope furrow with total length 30 m is first presented. The furrow cross section is trapezoidal with $B_0 = 0.17$ m, $Z = 1.2$, $H = 0.27$ m and $W = 1$ m. A low retention capacity soil (0.06 m) is assumed with a roughness Gauckler-Manning $n = 0.015$ m s$^{-1/3}$ and infiltration parameters $K = 0.0032$ m s^{-a}, $a = 0.42$ and $f_0 = 0$ m s^{-1}. The water inlet point is located at the upstream end ($l = 0$ m) whereas the fertilizer inlet point is assumed at $l = 1$ m. In all the scenarios 0.9 m^3 of water are applied as well as 0.9 kg of fertilizer with a solubility $S = 10$ kg m^{-3}. The fertilizer is applied at a constant rate but during application times of different duration. The final irrigation time (t_s) used is the one required for the total infiltration of the surface water. The discretization parameters are the grid size $\delta l = 1$ m and the time step that is ruled by the CFL = 0.9 in all the simulations. The computational time spent in the 9 scenarios has been 0.37 s on a desktop PC with Intel Core i5 3.2 GHz processor without any parallelization.

Table 3 contains the detail of the different inlet discharge values as well as the initial (t_i) and final (t_f) application times. The final irrigation time and the distribution uniformity results are also included. Figure 12 is the plot of the longitudinal profile of infiltrated water and solute. Better uniformity values are obtained with larger inlet discharges. The application of the fertilizer 1 m away from the water inlet point reduces the fertilizer uniformity as the fertilizer infiltration upstream the application point is negligible. The distributed fertilizer application strategies (in scenarios 2, 5 an 8 it is applied during the first half-period whereas in scenarios 3, 6 and 8 it is applied during the second half-period) reduce considerably the fertilizer uniformity in general.

Table 3: Final irrigation time, discharges, application times and water/fertilizer uniformity for scenarios 1-9.

		Water				Fertilizer			
Scenario	t_s s	Q_{in} m^3 s^{-1}	t_i s	t_f s	UW_{25} %	Q_{in} kg s^{-1}	t_i s	t_f s	UF_{25} %
1	1020	0.002	0	450	88.72	0.002	0	450	65.43
2	1020	0.002	0	450	88.72	0.004	0	225	42.39
3	1020	0.002	0	450	88.72	0.004	225	450	68.42
4	858	0.005	0	180	95.37	0.005	0	180	71.85
5	858	0.005	0	180	95.37	0.010	0	90	59.31
6	858	0.005	0	180	95.37	0.010	90	180	22.12
7	830	0.010	0	90	96.58	0.010	0	90	71.69
8	830	0.010	0	90	96.58	0.020	0	45	54.22
9	830	0.010	0	90	96.58	0.020	45	90	5.26

5.2. Simulation of 12 fertigation scenarios in a furrow network

This set of scenarios (10 to 21) is concerned with the simulation in a plot 120 m x 200 m with a network of 120 irrigation furrows. A low infiltration soil with the Kostiakov-Lewis parameters $K = 1.0 \cdot 10^{-3}$ m s^{-a}, $a = 0.2$ and $I_c = 1.0 \cdot 10^{-6}$ m s^{-1} is assumed. The roughness model (10) has been used

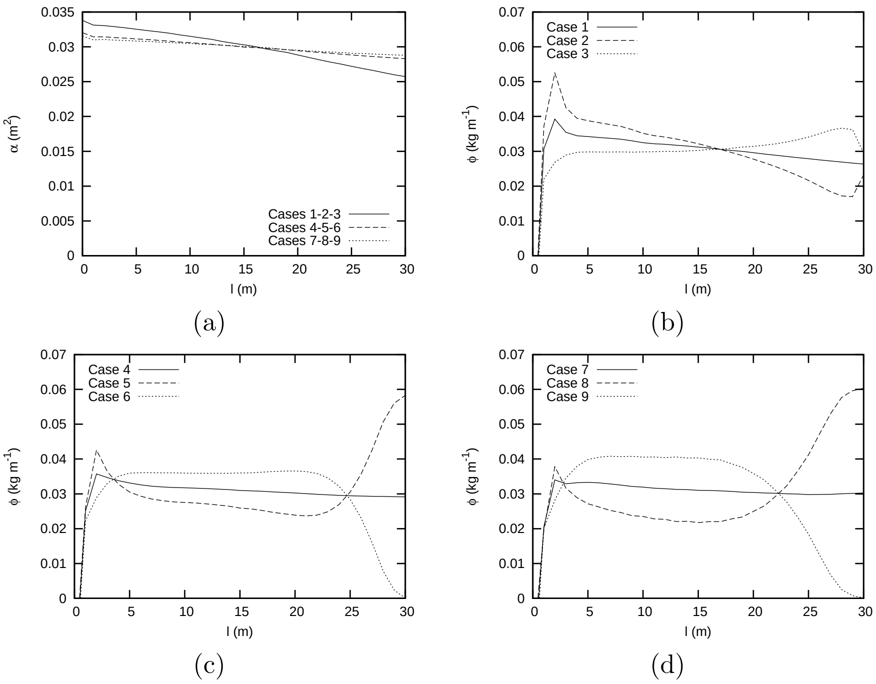

Figure 12: Longitudinal profiles of volume of water (a) and mass of solute (b, c and d) infiltrated per unit length of furrow for the scenarios 1-9.

with the typical furrow values $\epsilon = 0.03$ and $d = 0.02$ m. The irrigation furrows are assumed of trapezoidal cross section given by $B_0 = 0.17$ m, $Z = 1.67$, $H = 0.20$ m, $W = 1$ m and with a longitudinal slope $S_0 = 0.0001$. Level distribution and recirculation furrows are assumed ($S_0 = 0$) with a cross section given by $B_0 = 0.37$ m, $Z = 1.67$, $H = 0.25$ m and $W = 1.2$ m. A total water volume of 2160 m^3 and 1080 kg fertilizer with solubility $S = 1$ kg m^{-3} are applied during 20 hours. In scenarios 10-13 water is applied at an extreme point in the distribution furrow. In scenarios 14-17 it is applied at the mid-point of the distribution furrow and in scenarios 18-21 water is applied simultaneously at the two end points of the distribution furrow. On the other hand, in scenarios 10, 14 and 18 the fertilizer is applied during 20 hours, in scenarios 11, 15 and 19 it is applied during the first 10 hours and in scenarios 12, 16 and 20 it is applied in the last 10 hours. In all scenarios, water and fertilizer are applied at the same location except in scenarios 13, 17 and 21, where the fertilizer is applied suddenly at the beginning time on 9 equally distributed points along the distribution furrow. Figures 13 and 14, and table 4, show the sketch of the water and fertilizer application in the different scenarios.

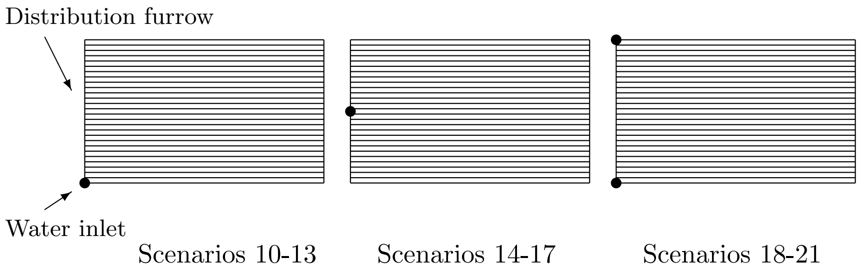

Figure 13: Water application in scenarios 10-21.

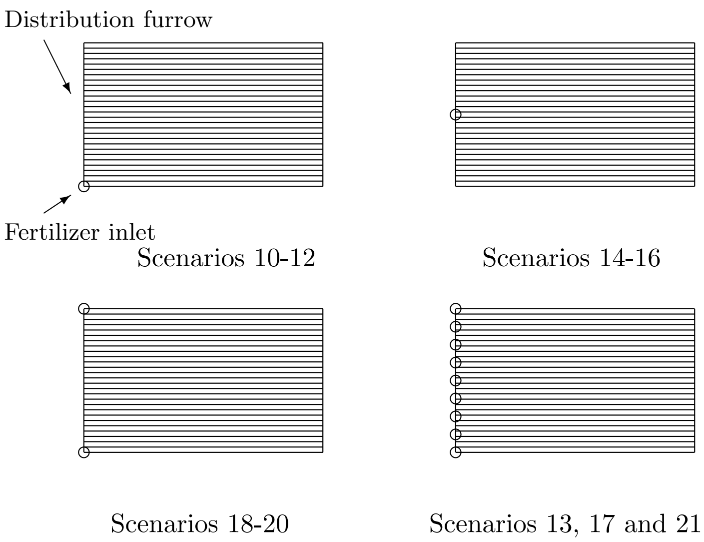

Figure 14: Fertilizer application in scenarios 10-21.

In all cases, the total irrigation lifetime required by complete infiltration of surface water takes about 46-47 hours. For the numerical simulation, a grid spacing $\delta l = 1$ m was used in all scenarios, leading to 24480 cells. The time step was controlled by CFL = 0.9.

Figure 15 shows a snapshot of the program with a distribution map of the surface water depth in scenario 10 at $t = 43200$ s.

Table 4: Water and fertilizer applications for scenarios 10-21.

	Water				Fertilizer			
Scenario	t_i h	t_f h	Inlets number	Inlets location	t_i h	t_f h	Inlets number	Inlets location
10	0	20	1	Corner	0	20	1	Corner
11	0	20	1	Corner	0	10	1	Corner
12	0	20	1	Corner	10	20	1	Corner
13	0	20	1	Corner	Suddenly at $t = 0$		9	Distributed
14	0	20	1	Middle	0	20	1	Middle
15	0	20	1	Middle	0	10	1	Middle
16	0	20	1	Middle	10	20	1	Middle
17	0	20	1	Middle	Suddenly at $t = 0$		9	Distributed
18	0	20	2	Corners	0	20	2	Corners
19	0	20	2	Corners	0	10	2	Corners
20	0	20	2	Corners	10	20	2	Corners
21	0	20	2	Corners	Suddenly at $t = 0$		9	Distributed

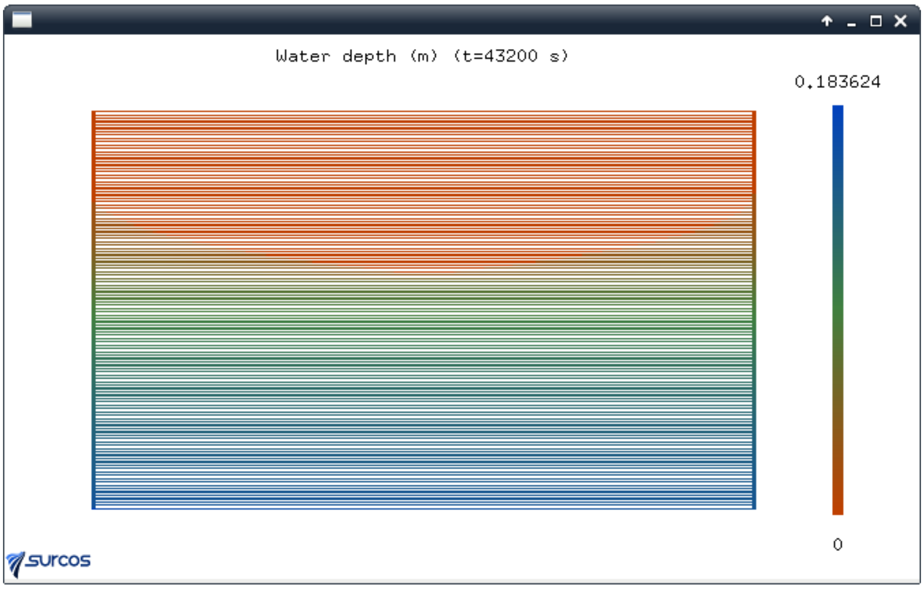

Figure 15: Map of the water depth for scenario 10 at $t = 43200$ s as displayed by the program *surcos*.

Figure 16 shows a snapshot of the program with the longitudinal surface and infiltrated water depth profiles in the 60th furrow for scenario 10 at $t = 3240$ s.

Figure 17 shows a snapshot of the program with the time evolution of the surface water depth and concentration at a point located in the mid point of the distribution furrow for scenario 10.

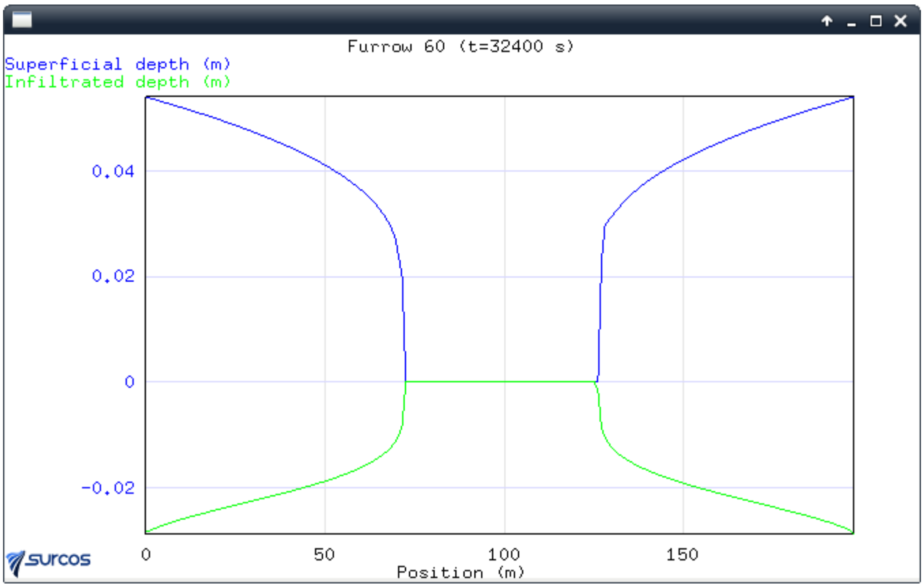

Figure 16: Longitudinal profile of the surface and infiltrated water in the 60th irrigation furrow for the scenario 10 at $t = 32400$ s displayed by the program *surcos*.

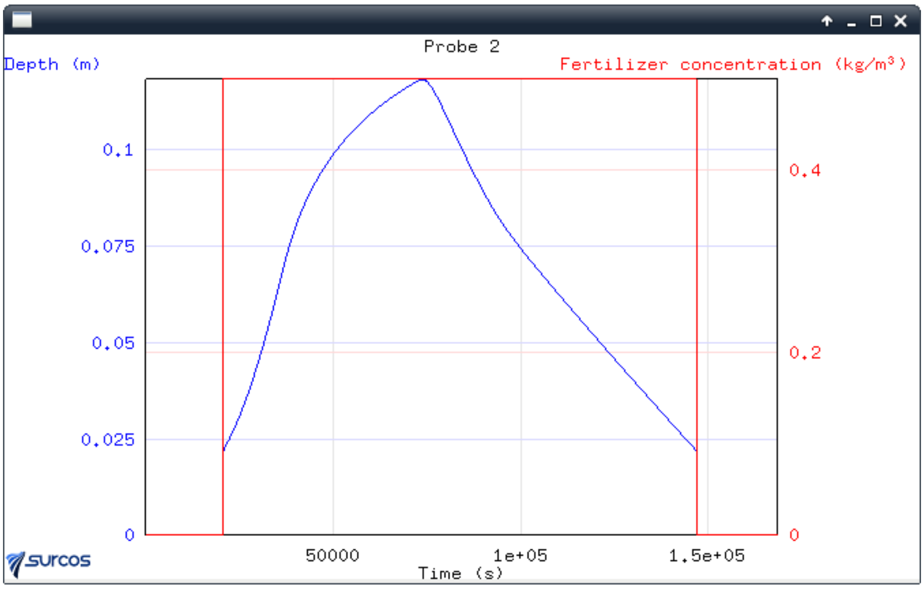

Figure 17: Time evolution at a probe located at the center of the distribution furrow for scenario 10 as displayed by the program *surcos*.

Table 5 presents the irrigation times as well as water and fertilizer efficiency and uniformity achieved for scenarios 10-21. The water application efficiency is excellent in all cases, with a zero percolation flow. The fertilizer application efficiency is also excellent except in scenarios 13, 17 and 21 where some of the fertilizer is not dissolved. The water distribution uniformity is good ($> 76\%$) and improves when the inlet is located at the distribution furrow midpoint or end points ($\approx 87\%$). The fertilizer distribution uniformity is also good when it is applied together with water (scenarios 10, 14 and 18). The fractional application of the fertilizer in the first or second half of the application time reduces the uniformity. It is worth noting that the strategy of spatial fertilizer distribution along 9 points in the distribution furrow not only reduces efficiency, due to the non-dissolved solid fraction, but also produces a loss in uniformity in these scenarios.

Table 5: Final irrigation times as well as water and fertilizer efficiency and uniformity achieved for scenarios 10-21.

		Water		Fertilizer	
Scenario	t_s hh:mm	EW %	UW_{25} %	EF %	UF_{25} %
10	46:39	98.58	76.86	98.58	**76.86**
11	46:39	98.58	76.86	98.91	4.77
12	46:39	98.58	76.86	98.01	10.33
13	46:39	98.58	76.86	74.47	1.81
14	46:19	98.55	87.37	98.55	**87.37**
15	46:19	98.55	87.37	98.78	34.08
16	46:19	98.55	87.37	98.31	33.63
17	46:19	98.55	87.37	65.51	0.97
18	46:19	98.55	87.34	98.55	**87.34**
19	46:19	98.55	87.34	98.79	33.27
20	46:19	98.55	87.34	98.14	32.90
21	46:19	98.55	87.34	74.13	0.22

The time used by a 2.8 GHz Intel Core i7 desktop computer to run the 12 scenarios in four parallel processes, in order to do an optimal use of the four CPU cores, was 14 h : 02 min, about one hour per simulation.

6. Conclusions

This work has presented program *surcos*. The core of the program is a well tested mathematical model including shallow water flow and solute transport solved using a second order TVD scheme. The verification and validation of the numerical model can be found in previous publications (Burguete et al., 2009a,b). The model is adapted to furrow fertigation and implements an infiltration equation that automatically adjusts to variations in the wetted perimeter, a roughness equation based on an absolute roughness parameter, and an equation for the estimation of the longitudinal diffusion parameter. The model also incorporates a specific treatment of the boundary conditions formulated to ensure perfect global mass conservation. The model goes eyond furrow irrigation and fertigation to furrow networks by means of a simple and computationally efficient approach to the junction conditions, considered as internal boundaries.

Numerical tests have been used to assess the model properties for the calculation of both water level and solute concentration front advance, and to evaluate the performance of the treatment of boundary conditions and junctions. The results of these tests have confirmed the adequacy of the model to address the problems of unsteady flows with solute transport in single channels and junctions in channels.

The model shows very adequate for the prediction of both water movement and infiltration as well as fertilizer transport. Several water and fertilizer application points and times have been used in order to prove the applicability of the model in a level furrow network. All the simulations lead to numerical results that are characterized by lack of numerical oscillations and perfect water volume conservation. The analysis of the different cases leads to the main conclusion that it works well, it is reliable, fast and very easy to use. This program can be a useful tool for the optimization of surface irrigation and fertigation in furrows and furrow networks.

The present model *surcos* improves previous developments by offering the possibility to model water flow and solute transport in furrow junctions and furrow networks. The model and the examples presented in this work are distributed (Burguete et al., 2013a,b) as free software under a BSD type license with available and editable source code.

Notation

α = volume of water infiltrated per unit length of furrow,

Δ = time increment,

δ = spatial increment,

δw_k = first order upwind coefficients,

ϵ = dimensionless parameter of aerodynamical resistance,

θ = parameter controlling the degree of implicitness of the source term,

$\mathbf{\Lambda}$ = flow Jacobian eigenvalues diagonal matrix,

λ^k = flow Jacobian eigenvalues,

ν = artificial viscosity coefficient,

ϕ = mass of solute infiltrated per unit length of the furrow,

$\Psi_k^{\pm}$ = high order TVD coefficients,

ψ = high order TVD flux limiter function,

A = wetted cross sectional area,

a = Kostiakov model exponent,

B = cross section top width,

B_0 = furrow base width,

b = fitting exponent of the vertical profile of flow velocity,

CFL = dimensionless Courant-Friedrichs-Lewy number,

c = velocity of the infinitesimal waves,

$\vec{D}$ = solute dispersion vector,

d = characteristic length of the bed roughness irregularities,

EF = fertilizer efficiency,

EW = water efficiency,

$\vec{F}$ = flux vector,

$G_k^{\pm}$ = first order upwind coefficients,

g = gravity constant,

H = furrow depth,

h = water depth,

h_{min} = depth threshold value to allow water discharge,

I = infiltration rate,

$\vec{I}$ = infiltration vector,

I_1 = pressure force integral,

I_c = saturated infiltration long-term rate,

$\mathbf{J}$ = Jacobian matrix of the flow,

K = Kostiakov model constant,

K_l = longitudinal solute dispersion coefficient,

L = furrow length,

$L_k^{\pm}$ = high order TVD coefficients,

l = longitudinal coordinate,

$M_{junction}$ = total mass of solute at the junction cells,

m_i = solid mass deposed at i-th cell,

N = number of cells discretizing a furrow,

$o_k^{\pm}$ = first order upwind coefficients,

P = cross-sectional wetted perimeter ,

$\mathbf{P}$ = flow Jacobian diagonalizer matrix,

Q = discharge,

Q_{in} = inflow discharge,

R = water retention capacity of the soil,

$R_k^{\pm}$ = high order TVD coefficients,

r = friction factor,

$\vec{r}_{in}$ = inflow point location vector,

S = fertilizer instantaneous solubility,

S_0 = longitudinal bottom slope,

$\vec{S}^c$ = source term vector,

S_f = longitudinal friction slope,

s = cross sectional average solute concentration,

t = time,

t_f = final application time,

t_i = initial application time,

t_s = final irrigation time required to complete infiltration,

$\vec{U}$ = vector of conserved variables,

UF_{25} = fertilizer low quarter uniformity,

UW_{25} = water low quarter uniformity,

u = cross sectional average velocity,

$V_{junction}$ = total volume of water at the junction cells,

W = distance between furrows,

y = transversal coordinate,

Z = tangent of the angle between the furrow walls and the vertical direction,

z = vertical coordinate,

z_b = bed level,

z_s = surface water level.

Bautista, E., Clemmens, A. J., Strelkoff, T. S., Niblack, M., 2009a. Analysis of surface irrigation systems with WinSRFR – example application. Agricultural Water Management 96 (7), 1162–1169.

Bautista, E., Clemmens, A. J., Strelkoff, T. S., Schlegel, J., 2009b. Modern analysis of surface irrigation systems with WinSRFR. Agricultural Water Management 96 (7), 1146–1154.

Burguete, J., García-Navarro, P., 2001. Efficient construction of high-resolution TVD conservative schemes for equations with source terms: application to shallow water flows. International Journal for Numerical Methods in Fluids 37 (2), 209–248.

Burguete, J., García-Navarro, P., 2004. Implicit schemes with large time steps for non-linear equations: application to river flow hydraulics. International Journal for Numerical Methods in Fluids 46 (6), 607–636.

Burguete, J., García-Navarro, P., Murillo, J., 2006. Numerical boundary conditions for globally mass conservative methods to solve the shallow-water equations and applied to river flow. International Journal for Numerical Methods in Fluids 51 (6), 585–615.

Burguete, J., García-Navarro, P., Murillo, J., 2007a. Preserving bounded and conservative solutions of transport in 1D shallow-water flow with upwind numerical schemes: application to fertigation and solute transport in rivers. International Journal for Numerical Methods in Fluids 56 (9), 1731–1764.

Burguete, J., García-Navarro, P., Murillo, J., 2008. Friction term discretization and limitation to preserve stability and conservation in the 1D shallow-water model: application to unsteady irrigation and river flow. International Journal for Numerical Methods in Fluids 58 (4), 403–425.

Burguete, J., García-Navarro, P., Murillo, J., García-Palacín, I., 2007b. Analysis of the friction term in the one-dimensional shallow water model. ASCE Journal of Hydraulic Engineering 133 (9), 1048–1063.

Burguete, J., Lacasta, A., García-Navarro, P., 2013a. SURCOS: a program to calculate fertirrigation in isolated furrows and furrow networks (execute files, manuals and examples). URL http://digital.csic.es/handle/10261/75830.

Burguete, J., Lacasta, A., García-Navarro, P., 2013b. SURCOS: a program to calculate fertirrigation in isolated furrows and furrow networks (source code). URL https://github.com/jburguete/surcos.

Burguete, J., Zapata, N., García-Navarro, P., Maïkaka, M., Playán, E., Murillo, J., 2009a. Fertigation in furrows and level furrow systems. I: Model description and numerical tests. ASCE Journal of Irrigation and Drainage Engineering 135 (4), 401–412.

Burguete, J., Zapata, N., García-Navarro, P., Maïkaka, M., Playán, E., Murillo, J., 2009b. Fertigation in furrows and level furrow systems. II: Field experiments, model calibration, and practical applications. ASCE Journal of Irrigation and Drainage Engineering 135 (4), 413–420.

Clemmens, A. J., Strelkoff, T. S., 1999. SRFR, version 4.06. U.S. Water Consevation Laboratory. Agricultural Research Service, Phoenix.

Courant, R., Friedrichs, K. O., Lewy, H., 1928. Über die partiellen differenzengleichungen der mathematisches. Math. Ann. 100, 32–74.

Ebrahimiam, H., Liaghat, A., 2011. Field evaluation of various mathematical models for furrow and border irrigation systems. Soil and Water Research 6 (2), 91–101.

Gauckler, P. G., 1867. études théoriques et practiques sur l'écoulement et le mouvement des eaux. Comptes Rendues de l'Académie des Sciences, Paris.

Mailapalli, D. R., Singh, R., Raghuwanshi, N. S., 2009. Physically based model for simulating flow in furrow irrigation. I: Model development. ASCE Journal of Irrigation and Drainage Engineering 135, 739.

Manning, R., 1890. On the flow of water in open channels and pipes. Institution of Civil Engineers of Ireland.

Roe, P. L., 1981. Approximate Riemann solvers, parameter vectors, and difference schemes. Journal of Computational Physics 43 (2), 357–372.

Rutherford, J. C., 1994. River mixing. John Wiley & Sons.

Soroush, F., Fenton, J. D., Mostafazadeh-Fard, B., Mousavi, S. F., Abbasi, F., 2013. Simulation of furrow irrigation using the slow-change/slow-flow equation. Agricultural Water Management 116 (1), 160–174.

Walker, W. R., 2003. SIRMOD III, surface irrigation simulation software. Utah State University, Logan, Utah.

Walker, W. R., Skogerboe, G. V., 1987. Surface irrigation. Theory and practice. Prentice-Hall, Inc., Englewood Cliffs, New Jersey.